Feedback in the β-catenin destruction complex imparts bistability and cellular memory

Authors: Mary Jo Cantoria[1,2 †], Elaheh Alizadeh[1,2†], Janani Ravi[3,4], Nawat Bunnag[5], Arminja N. Kettenbach[6], Yashi Ahmed[5], Andrew L Paek[7], John J. Tyson[3], Konstantin Doubrovinski[8]*, Ethan Lee[9,10]*, Curtis A. Thorne[1,2]*

Affiliations:

[1]Department of Cellular and Molecular Medicine, University of Arizona, Tucson, AZ 85721, U.S.A.

[2]University of Arizona Cancer Center, Tucson, AZ 85724, U.S.A.

[3]Department of Biological Sciences, Virginia Polytechnic Institute & State University, Blacksburg, VA 24061, U.S.A.

[4]Current address: Department of Pathobiology and Diagnostic Investigation, Microbiology and Molecular Genetics, Michigan State University, East Lansing, MI 48824, U.S.A.

[5]Department of Molecular and Systems Biology and the Norris Cotton Cancer Center, Geisel School of Medicine at Dartmouth College, Hanover, NH 03755, U.S.A.

[6]Department of Biochemistry and Cell Biology and the Norris Cotton Cancer Center, Geisel School of Medicine at Dartmouth College, Lebanon NH 03756, U.S.A.

[7]Department of Molecular and Cellular Biology, University of Arizona, Tucson, AZ 85721, U.S.A.

[8]Green Center for Systems Biology, UT Southwestern Medical Center, Dallas, TX 75390, U.S.A.

[9]Department of Cell and Developmental Biology, Vanderbilt University, Nashville, TN 37232, U.S.A.

[10]Vanderbilt Ingram Cancer Center, Vanderbilt University Medical Center, Nashville, TN 37232, U.S.A.

† These authors contributed equally to this work

***Corresponding author: Email**: curtisthorne@email.arizona.edu, ethan.lee@vanderbilt.edu, Konstantin.Doubrovinski@utsouthwestern.edu

ABSTRACT

Wnt ligands are considered classical morphogens, for which the strength of the cellular response is proportional to the concentration of the ligand. Herein, we show an emergent property of bistability arising from feedback among the Wnt destruction complex proteins that target the key transcriptional co-activator β-catenin for degradation. Using biochemical reconstitution, we identified positive feedback between the scaffold protein Axin and the kinase GSK3. Theoretical modeling of this feedback between Axin and GSK3 predicted that the activity of the destruction complex exhibits bistable behavior. We experimentally confirmed these predictions by demonstrating that cellular cytoplasmic β-catenin concentrations exhibit an "all-or-none" response with sustained memory (hysteresis) of the signaling input. This bistable behavior was transformed into a graded response and memory was lost through inhibition of GSK3. These findings provide a mechanism for establishing decisive, switch-like cellular response and memory upon Wnt pathway stimulation.

One Sentence Summary:

Positive feedback within the β-catenin destruction complex gives rise to bistability and memory in response to Wnt stimulation, imparting signal transduction accuracy and insulation.

RESULTS

Wnt/β-catenin signaling is involved in organism development, stem cell maintenance and is misregulated in human disease. At the core of this signaling pathway is the β-catenin destruction complex, comprised of the kinases glycogen synthase kinase 3 (GSK3) and casein kinase 1 alpha (CK1α), and the scaffolding proteins Axin and Adenomatous polyposis coli (APC). In the absence of Wnt ligands, phosphorylation of the transcriptional co-activator β-catenin within the destruction complex targets β-catenin for ubiquitin-mediated proteasomal degradation, thereby maintaining low levels of cytoplasmic and nuclear β-catenin. Wnt signaling inhibits phosphorylation of β-catenin to block its turnover; accumulated β-catenin subsequently enters the nucleus to mediate a Wnt-specific transcriptional program required for animal development and tissue homeostasis (*1*).

Although Wnt ligands are considered classical morphogens, Wnt gradients are dispensable for proper patterning during development in some contexts (*2-4*). To better understand the biochemical function of the β-catenin destruction complex and to assess how critical steps within the complex impact behavior of the Wnt pathway, we performed biochemical reconstitutions of the destruction complex with Xenopus egg extracts and purified proteins. Based on these measurements, we developed mathematical simulations of destruction complex dynamics and validated our model by performing single-cell analyses of β-catenin behavior.

Previous studies in cultured mammalian cells and *in vitro* reconstitution have shown that the scaffold protein Axin is a direct target of GSK3 (*5, 6*). Because *Xenopus* egg extracts are

readily amenable to biochemical studies and faithfully recapitulate signaling dynamics that control β-catenin turnover (*7*), we examined the regulation of Axin by GSK3 in extracts (Fig. 1A). Consistent with previous studies (*5*), inhibition of GSK3 with LiCl induced Axin turnover (Fig. 1B,C). Stabilization of Axin required both the GSK3 phosphorylation sites at serine 322 and serine 326, and the GSK3 binding site (GBS) on Axin (Fig. 1C) (*8*).

As Axin is the limiting component of the destruction complex, overexpression of Axin promotes β-catenin degradation and inhibits Wnt signaling even in the absence of APC (*9, 10*). The limiting concentration of Axin provides a simple means for insulating a discrete pool of GSK3 that specifically targets β-catenin for phosphorylation (*10*). In addition, given its role as a scaffold, Axin is ideally positioned to regulate the activity of GSK3, thereby promoting both Axin stability and β-catenin degradation. We initially examined GSK3 activity in *Xenopus* egg extracts using a phospho-specific antibody that recognizes GSK3β phosphorylation at serine 9 (pS9 GSK3), which limits GSK3β activity. The addition of recombinant Axin to extracts resulted in a marked reduction in pS9 GSK3 (Fig. 1D). The requirement for a phosphatase in β-catenin degradation has been reported (*11*). Thus, we tested the effect of the phosphatase inhibitor okadaic acid (OA) on pS9 GSK3. We found that OA prevented the Axin-mediated reduction of pS9 GSK3 in *Xenopus* extracts (Fig. 1D), suggesting an OA-sensitive phosphatase requirement at this regulatory step.

To identify Axin regions that bind co-factors necessary for pS9 GSK3 dephosphorylation, we performed domain deletion analysis by expressing Axin mutants in HEK 293 cells (Fig. 1E).

As expected, full-length Axin promoted loss of the inhibitory phosphorylation of GSK3, and OA blocked this effect, suggesting phosphatase dependence of GSK3 activation. Similarly, the deletion of the GSK3 binding site (GBS) or the phosphatase 2A (PP2A) domains of Axin prevented Axin-mediated inhibition of GSK3 phosphorylation, suggesting these regions are essential for GSK3 activation by Axin. In contrast, Axin lacking its β-catenin binding site (βcat-BS), APC binding site (RGS), or DIX domain still promoted the removal of the inhibitory serine 9 phosphorylation on GSK3; thus, these sites are not required for Axin-mediated removal of serine 9 phosphorylation on GSK3. Additionally, Axin was recently shown to contain a short linear motif (SLiM) that interacts with the B56 subunit of PP2A (*12, 13*). We made alanine mutants of this conserved SLiM sequence (Fig. S1) and found that SLiM 4A Axin mutants could not remove pS9 on GSK3 (Fig. 1F).

To test if PP2A could directly act on pS9 GSK3, we performed *in vitro* reconstitution using purified components of the destruction complex. We found that PP2A exhibited a preference for pS9 GSK3 (Fig. 1G) versus the β-catenin sites phosphorylated by GSK3 (phospho-serine 33, serine 37, and threonine 41; Fig. 1H). Based on these findings, we propose the following model: the majority of cytoplasmic GSK3 is in or fluctuating as the pS9 GSK3 state, which normally limits its activity. Upon pS9 GSK3 binding to Axin, pS9 GSK3 is targeted for dephosphorylation by Axin-bound PP2A. Dephosphorylated GSK3 is active and phosphorylates Axin to promote its stabilization. Active, dephosphorylated GSK3 and phosphorylated Axin (bound to APC) comprise

a destruction complex state that is "fully activated" to phosphorylate β-catenin, targeting it for ubiquitin-mediated proteasomal degradation.

We built a theoretical model based on our biochemical observations to better understand the reaction kinetics within the β-catenin destruction complex (Fig. 2A). GSK3 concentration was kept constant as it is predicted to be degraded at a relatively slow rate (*10*). Rates of Axin synthesis and degradation were based on our *Xenopus* extract data and previous work (*10*). We translated our model (Fig. 2A) into a set of ordinary differential equations (ODEs) (TableS1) and solved them numerically and analytically in steady-state conditions (Fig. S2). The reaction rates and rate constants used in the model are listed in Table S2 and Table S3, respectively. As shown in Fig. 2A, our model showed a positive feedback loop between Axin and GSK3.

The function of the destruction complex is to promote the phosphorylation and subsequent ubiquitin-mediated degradation of β-catenin. When $Axin^P$ and GSK3 are high, β-catenin is low, and the pathway is "off." When $Axin^P$ and GSK3 are low (e.g., via Wnt activation), cytoplasmic and nuclear β-catenin is high, and the pathway is "on." Consistent with previous work, we modeled the Wnt signal to act on the active, destruction complex-bound GSK3 by directly increasing the inhibitory rate (k_1) (*14*) and calculated the steady-state concentration of β-catenin. To model pathway activation, we started initially with a low value of k_1, which was followed by a gradual increase. For each k_1 value, the β-catenin concentration was determined and plotted as "naive." Additionally, we solved the equations with decreasing values of k_1, starting with a high value, and

referred to this as "pre-activated." As shown in Fig. 2B, for a range of $k_1<0.85$, we found that the Wnt signal strength needed to stabilize β-catenin from the naive state was higher than the signal strength needed to maintain β-catenin once the system had been pre-activated. In contrast, when dephosphorylation of GSK3 by $Axin^P$ was omitted from the model, the effect of k1 was identical for "naïve" and "pre-activated" states (Fig. 2C).

Our modeling suggests the β-catenin destruction complex has two stable states, “off” and “on”. This bistability may result from self-perpetuating states such as positive feedback or double-negative feedback (*15*). A bistable system is characterized by two alternative steady states, an off-state and an on-state, without intermediate states (Fig. 3A) (*15*). In a population of cells, the inflection point of the switching will be set by subtle variation in the concentrations and rates of pathway components. This is why, in a uniform sheet of cells, one often observes a salt-and-pepper phenotype rather than perfect collective switching. To simulate the heterogeneous response of a population of cells, we ran the simulation for 2,000 cells where we randomly selected a k_1 value for each cell from a normal distribution (Fig. S3). We then plotted the distribution of β-catenin with an increase in the mean value of k_1 (Fig. 3B) that demonstrates the expectation for β-catenin response in a noisy tissue culture system.

We then validated whether the positive feedback between Axin and GSK3 observed in *Xenopus* egg extracts can lead to a bistable response in mammalian cells activated by Wnt ligands. Accurate single-cell quantification of soluble β-catenin has been challenging due to the high

concentrations of non-signaling β-catenin at adherens junctions. We combined automated imaging with custom cell-identification software (Fig. 3C) to analyze primary, immortalized human colonic epithelial cells (HCECs) (*16*). By varying concentrations of purified, recombinant Wnt3a, and measuring nuclear β-catenin, we found that at low Wnt3a concentrations, signaling is in the off-state (nuclear β-catenin is absent), whereas, at high Wnt concentrations, signaling is in the on-state (nuclear β-catenin is present) (Fig. 3D). At intermediate Wnt3a doses, we found a mixed population of cells that were either in the off- or the on-state, with a bistable range between 2 and 6 nM Wnt3a. The β-catenin response to increasing Wnt3a exhibited a Hill-coefficient of ~6, suggesting cooperativity among responding factors (Fig. S4).

For a system to be genuinely bistable, it must exhibit hysteresis, i.e., the concentration of Wnt needed to induce a given response (after Wnt exposure) is lower than the concentration of Wnt required to mediate the initial response (*15*). An alternative possibility for the salt-and-pepper β-catenin phenotype we observed is the existence of a monostable transcritical bifurcation, a mechanism often found in phase separation settings, in which a two-state system switches states at a single inflection point (i.e., turning on and turning off occur at the same ligand concentration) (*17*). To test this, we fully activated cells with high concentrations of Wnt ligand and then measured the concentrations of Wnt needed to maintain the on-state (Fig. 4A). We observed that cells that were previously treated with a high concentration of Wnt maintained nuclear β-catenin

164 throughout the experiment (Fig. 4B,C) and that this hysteretic behavior persisted several hours
165 after the initial Wnt3a treatment (Fig. S5, S6A).

166 We next tested whether the bistable response observed in HCEC cells in response to Wnt3a
167 treatment was due to positive feedback between Axin and GSK3 revealed in our biochemical
168 experiments (Fig. 1). Our modeling suggested bistability was lost by removing the function of
169 $Axin^{p}$ in the dephosphorylation of GSK3 (Fig. 5A,B). Wnt ligand-mediated activation of the Wnt
170 pathway occurs via a mechanism involving inhibition of GSK3-mediated β-catenin
171 phosphorylation (*14, 18, 19*). We predict, however, that direct inhibition of GSK3 with a small
172 molecule inhibitor that targets its ATP catalytic pocket would break the biochemical GSK3/Axin
173 feedback loop by being insensitive to $Axin^{p}$-dependent dephosphorylation of pS9 GSK3 (Fig. 5C).
174 We treated HCEC cells with the GSK3 inhibitor CHIR99021 (GSK3i) (*20*) and found that, in
175 contrast with the Wnt3a treatment regimen, activation of the pathway with GSK3i treatment failed
176 to promote the bistable behavior of nuclear β-catenin (Fig. 5D). Unlike Wnt3a, the effects of
177 GSK3i on β-catenin nuclear accumulation were readily reversible, and the nuclear β-catenin signal
178 was lost rapidly (without any observable evidence of hysteresis) after the removal of GSK3i (Fig.
179 S6B). Hence, for all GSK3i experiments, we used time points for which we observed a steady-
180 state response after GSK3i treatment, i.e., a minimum of 6 hours treatment (Fig. S7A), but we
181 could not wash out the inhibitor because β-catenin levels rapidly reset to baseline (Fig. S7B).
182 Finally, we observed that GSK3i caused cells to respond in a monostable, graded manner (Fig. 5D,

S8). These experimental findings further support the conclusion from our biochemical reconstitution and mathematical model: bistability and hysteresis in Wnt signaling are driven by positive feedback between Axin and GSK3.

DISCUSSION

These experiments demonstrate that a biochemical feedback loop between GSK3 and Axin maintains the β-catenin destruction complex in a stable off- or on-state. This switch-like behavior requires the mutual regulation of GSK3 and Axin via antagonistic behaviors of an additional kinase and phosphatase. We also provided evidence that the PP2A phosphatase acts on GSK3 to remove the inhibitory phosphorylation on serine 9. Modeling of these biochemical events predicted that cells would respond in a binary manner to Wnt pathway stimulation, which was supported by our experiments in human colonic epithelial cells. Additionally, these cells displayed memory to Wnt stimulation, and β-catenin remained in the nucleus even after Wnt ligands had been removed. These results suggest the β-catenin destruction complex displays robustness by existing in two self-sustaining attractor states of active and inactive, which provides a mechanism for suppressing potentially deleterious fluctuations in concentrations and activities of pathway components.

Bistability has emerged as a foundational principle in signal transduction (*21*), yet its existence has been elusive in the Wnt pathway. Beyond suppressing noise within the Wnt pathway, positive feedback in the β-catenin destruction complex provides a mechanism to insulate a pool of GSK3 required in the complex from the total cellular GSK3, thereby preventing crosstalk with

other GSK3-regulating pathways such as PI3K/AKT and MAPK (*22, 23*). Furthermore, the existence of both bistable and graded responses could explain why long-range Wnt morphogen activity is dispensable in certain in vivo contexts but essential in others(*24*). The phenomena described herein shed light on a foundational structure of the Wnt/β-catenin pathway that instills robustness and, when perturbed, could lead to vulnerabilities in the accurate processing of Wnt signals.

Acknowledgments: We are grateful to Dr. Jerry Shay of U.T. Southwestern Medical Center for providing us with the HCEC line. Funding: M.J.C. was supported by the Cancer Biology Training Grant CA T32009213-40. E.A. was supported by The Sidney Hopkins, Mayola B. Vail, and Patricia Ann Hanson Postdoctoral Fellowship. This work was supported by NIH grants GM122516 (E.L.) and CA224188 (E.L. and Y.A.), GM136233 (Y.A.), GM119455 (A.N.K.), DK103126 (C.A.T.), GM134207 (K.D.), and Robert A. Welch Foundation I-1950-20180324. (K.D.)

Author contributions: Conceptualization, C.A.T., E.L., and K.D. Investigation, M.J.C., E.A., J.R., J.J.T., N.B, A.N.K., Y.A., K.D., E.L., C.A.T.; Writing first draft, M.J.C., C.A.T., E.A., E.L. K.D.; All authors edited the manuscript and approved final submission; Supervision, C.A.T., E.L., and K.D.; Funding acquisition, C.A.T., E.L., and K.D. **Competing interests**: None.

References:

1. R. Nusse, H. Clevers, Wnt/beta-Catenin Signaling, Disease, and Emerging Therapeutic Modalities. *Cell* **169**, 985-999 (2017).
2. C. Alexandre, A. Baena-Lopez, J. P. Vincent, Patterning and growth control by membrane-tethered Wingless. *Nature* **505**, 180-185 (2014).
3. L. A. Baena-Lopez, X. Franch-Marro, J. P. Vincent, Wingless promotes proliferative growth in a gradient-independent manner. *Science signaling* **2**, ra60 (2009).

4. G. Morata, G. Struhl, Developmental biology: Tethered wings. *Nature* **505**, 162-163 (2014).
5. H. Yamamoto *et al.*, Phosphorylation of axin, a Wnt signal negative regulator, by glycogen synthase kinase-3beta regulates its stability. *The Journal of biological chemistry* **274**, 10681-10684 (1999).
6. K. Willert, S. Shibamoto, R. Nusse, Wnt-induced dephosphorylation of axin releases beta-catenin from the axin complex. *Genes Dev* **13**, 1768-1773 (1999).
7. A. Salic, E. Lee, L. Mayer, M. W. Kirschner, Control of beta-catenin stability: reconstitution of the cytoplasmic steps of the wnt pathway in Xenopus egg extracts. *Mol Cell* **5**, 523-532 (2000).
8. L. Ji *et al.*, The SIAH E3 ubiquitin ligases promote Wnt/beta-catenin signaling through mediating Wnt-induced Axin degradation. *Genes Dev* **31**, 904-915 (2017).
9. T. Nakamura *et al.*, Axin, an inhibitor of the Wnt signalling pathway, interacts with beta-catenin, GSK-3beta and APC and reduces the beta-catenin level. *Genes Cells* **3**, 395-403 (1998).
10. E. Lee, A. Salic, R. Kruger, R. Heinrich, M. W. Kirschner, The roles of APC and Axin derived from experimental and theoretical analysis of the Wnt pathway. *PLoS biology* **1**, E10 (2003).
11. J. M. Seeling *et al.*, Regulation of beta-catenin signaling by the B56 subunit of protein phosphatase 2A. *Science* **283**, 2089-2091 (1999).
12. E. P. T. Hertz *et al.*, A Conserved Motif Provides Binding Specificity to the PP2A-B56 Phosphatase. *Mol Cell* **63**, 686-695 (2016).
13. T. Kruse *et al.*, Mechanisms of site-specific dephosphorylation and kinase opposition imposed by PP2A regulatory subunits. *EMBO J* **39**, e103695 (2020).
14. C. S. Cselenyi *et al.*, LRP6 transduces a canonical Wnt signal independently of Axin degradation by inhibiting GSK3's phosphorylation of beta-catenin. *Proc Natl Acad Sci U S A* **105**, 8032-8037 (2008).
15. J. E. Ferrell, Jr., Self-perpetuating states in signal transduction: positive feedback, double-negative feedback and bistability. *Curr Opin Cell Biol* **14**, 140-148 (2002).
16. A. I. Roig *et al.*, Immortalized epithelial cells derived from human colon biopsies express stem cell markers and differentiate in vitro. *Gastroenterology* **138**, 1012-1021 e1011-1015 (2010).
17. J. G. Albeck, J. M. Burke, S. L. Spencer, D. A. Lauffenburger, P. K. Sorger, Modeling a snap-action, variable-delay switch controlling extrinsic cell death. *PLoS biology* **6**, 2831-2852 (2008).
18. A. R. Hernandez, A. M. Klein, M. W. Kirschner, Kinetic responses of beta-catenin specify the sites of Wnt control. *Science* **338**, 1337-1340 (2012).
19. G. Wu, H. Huang, J. Garcia Abreu, X. He, Inhibition of GSK3 phosphorylation of beta-catenin via phosphorylated PPPSPXS motifs of Wnt coreceptor LRP6. *PLoS One* **4**, e4926 (2009).
20. F. H. Tran, J. J. Zheng, Modulating the wnt signaling pathway with small molecules. *Protein Sci* **26**, 650-661 (2017).
21. A. Goldbeter, Dissipative structures in biological systems: bistability, oscillations, spatial patterns and waves. *Philos Trans A Math Phys Eng Sci* **376**, (2018).

22. V. W. Ding, R. H. Chen, F. McCormick, Differential regulation of glycogen synthase kinase 3beta by insulin and Wnt signaling. *The Journal of biological chemistry* **275**, 32475-32481 (2000).
23. S. S. Ng *et al.*, Phosphatidylinositol 3-kinase signaling does not activate the wnt cascade. *The Journal of biological chemistry* **284**, 35308-35313 (2009).
24. R. A. Stewart, A. B. Ramakrishnan, K. M. Cadigan, Diffusion and function of Wnt ligands. *PLoS genetics* **15**, e1008154 (2019).
25. C. A. Thorne *et al.*, A biochemical screen for identification of small-molecule regulators of the Wnt pathway using Xenopus egg extracts. *J Biomol Screen* **16**, 995-1006 (2011).
26. C. R. Cabel *et al.*, Single-Cell Analyses Confirm the Critical Role of LRP6 for Wnt Signaling in APC-Deficient Cells. *Dev Cell* **49**, 827-828 (2019).

FIGURE LEGENDS

Fig. 1. GSK3 and Axin mutually activate in Xenopus extracts and mammalian cells.

(**A**) Experimental scheme. Cytoplasmic fraction of *Xenopus* egg extracts. Extracts are collected, spiked with radiolabeled (rad) [^{35}S] β-catenin or [^{35}S] Axin, and aliquots are removed at the indicated time points for analysis by SDS-PAGE and autoradiography. (**B**) Turnover of radiolabeled [^{35}S] β-catenin or [^{35}S]Axin in Xenopus extracts. LiCl (GSK3i) and NaCl (Control) (50 mM each) were added to extracts as indicated. (**C**) As in (B), turnover of Axin, AxinSA (serine 322 and 326 mutated to alanine), and AxinΔGBS (GSK3 binding site) in Xenopus extracts. (**D**) Axin promotes dephosphorylation of pS9 GSK3 in Xenopus extract, which is blocked by OA (200 nM). MBP-Axin (10 nM) was added to egg extract in the presence or absence of OA (10 nM), and pS9 GSK3 and GSK3 were detected by immunoblotting. (**E**) The β-catenin binding site, APC binding site, and DIX domain are dispensable for Axin-mediated dephosphorylation of pS9 GSK3. Myc-tagged Axin truncation mutants were transfected into HEK293 cells, as indicated, and immunoblotting was performed. For OA treatment, cells were incubated with 10 nM OA for 2 hrs prior to lysis. (**F**) Expression of FLAG-tagged wild-type Axin (Axin SLiM WT) and FLAG-tagged Axin with mutations in the conserved B56 binding site that prevent the interaction of B56 with Axin (Axin SLiM 4A) in HEK293. (**G**) Reconstitution of pS9 GSK3 dephosphorylation by PP2A in the presence of Axin. Recombinant Axin (1 μM) and GSK3 (10 μM) were incubated with ATP for 30 min to allow for the autophosphorylation of

GSK3. PP2A (1 μM) and OA (10 nM) were added for an additional 30 min, and samples were immunoblotted for pS9 GSK3. (**H**) PP2A preferentially dephosphorylates pS9 GSK3 versus β-catenin in the presence of Axin. The reaction was performed as in (F) but with the addition of β-catenin (10 μM).

Fig. 2. Mathematical modeling of the core β-catenin destruction complex components give rise to bistable Wnt activity. (**A**) Wiring diagram of β-catenin destruction complex feedback. Phosphorylated forms are denoted with "P." The model consists of a positive feedback loop between GSK3 and Axin^{P}. (**B**) We assume that an input Wnt signal changes the rate constant (k_1) in the phosphorylation flux of GSK3 (*18*). The model shows bistable response in β-catenin. **(C)** Bistability is lost when GSK3 is dephosphorylated by a phosphatase activity that is independent of Axin^{P}. Consequently , a graded β-catenin response is observed.

Fig. 3. Human colonic epithelial cells respond to Wnt in a bistable manner.

(**A**) Depiction of the difference between a graded versus a bistable response in an epithelial monolayer. (**B,D**) Density plots of nuclear β-catenin against Wnt concentrations in HCECs under simulated and experimental conditions show a bistable range of 3-6 nM Wnt3a. Steps of automated image processing to quantify nuclear β-catenin immunofluorescence signal. Inserts

show representative images of HCECs treated with Wnt at 6 hrs steady state. **(C)** Steps of automated image processing to quantify nuclear β-catenin immunofluorescence signal.

Fig. 4. Cells exhibit memory of Wnt stimulation.

(**A**) Scheme of the experimental approach to pre-stimulate colonic cells. (**B,C**) Model prediction of hysteresis and experimental results from Wnt3a dose-response analyses. Wnt3a dose-response density plots of nuclear β-catenin for HCECs treated with Wnt3a for the first time (naive) or previously pulsed with a high dose of Wnt3a (pre-stimulated). Results from simulated and experimental conditions are shown.

Fig. 5. Disrupting positive feedback removes bistability.

(**A**) Wiring diagram of β-catenin destruction complex feedback. GSK3i disrupts the positive feedback loop by removing the dependency of $Axin^{p}$ concentration on dephosphorylation of GSK3 (denoted by red X in the diagram) (**B**) CHIR00921 is epistatic to the Axin/PP2a regulation due to direct interaction with the ATP catalytic site on GSK3. (**C**) Model prediction of graded response and experimental results from CHIR009921 dose-response analyses. (**D**) GSK3 inhibition with CHIR99021 treatment results in a graded, monostable response in HCECs.

Figure 1

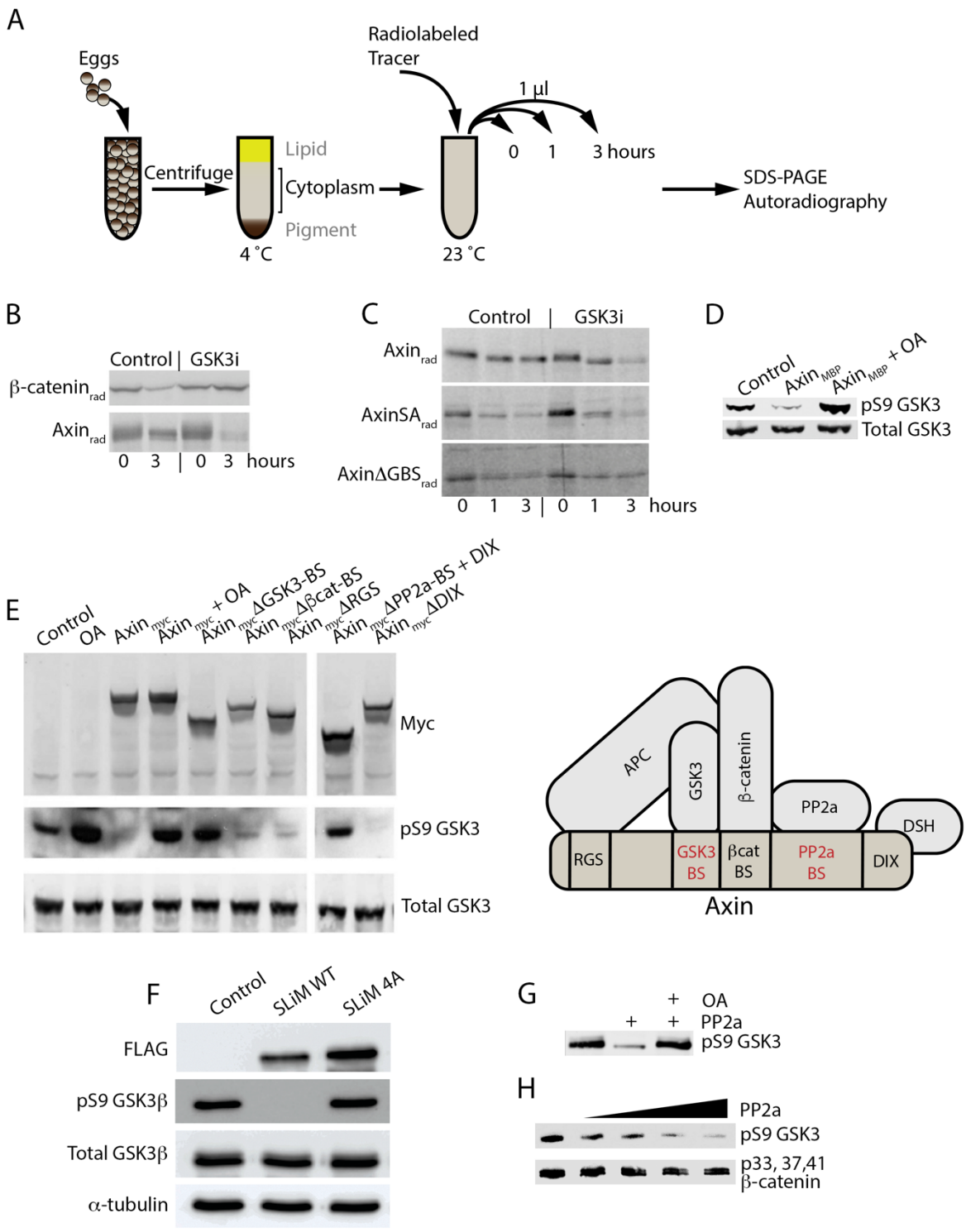

339

Figure 2

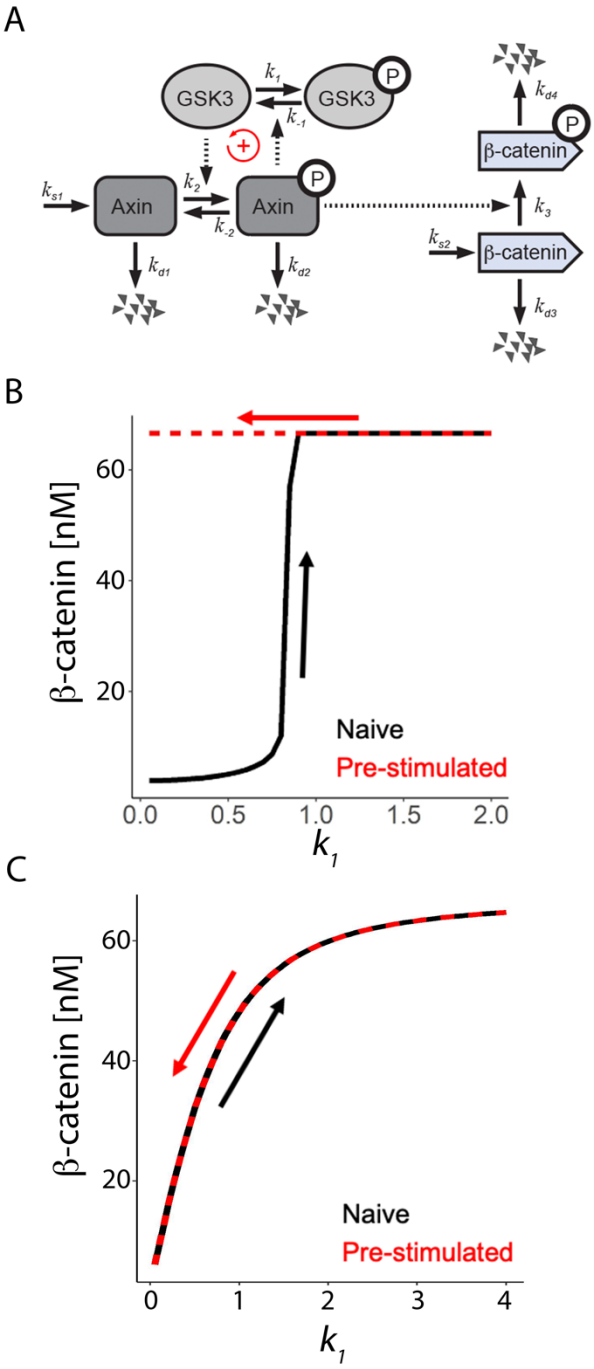

340

Figure 3

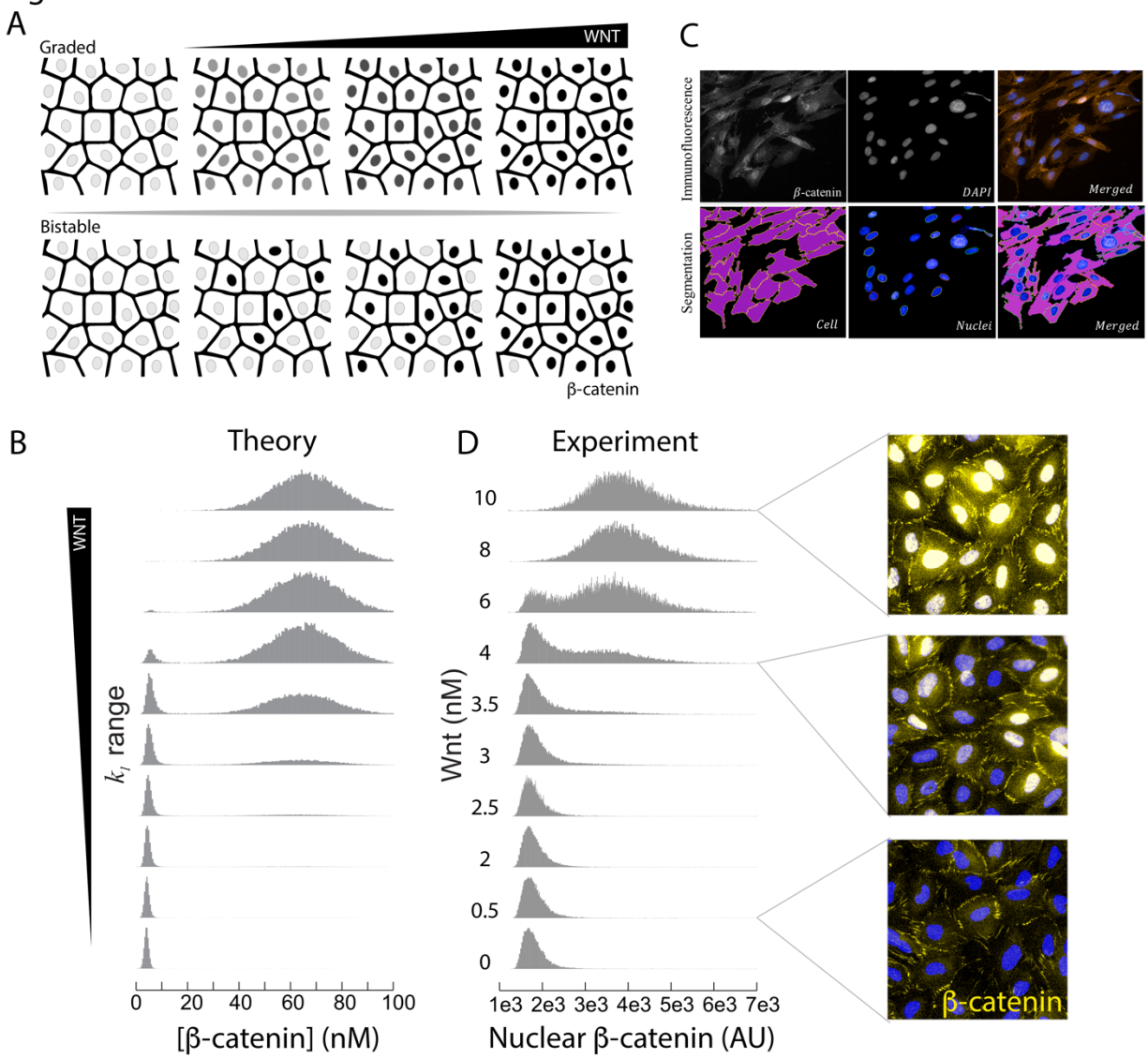

341

Figure 4

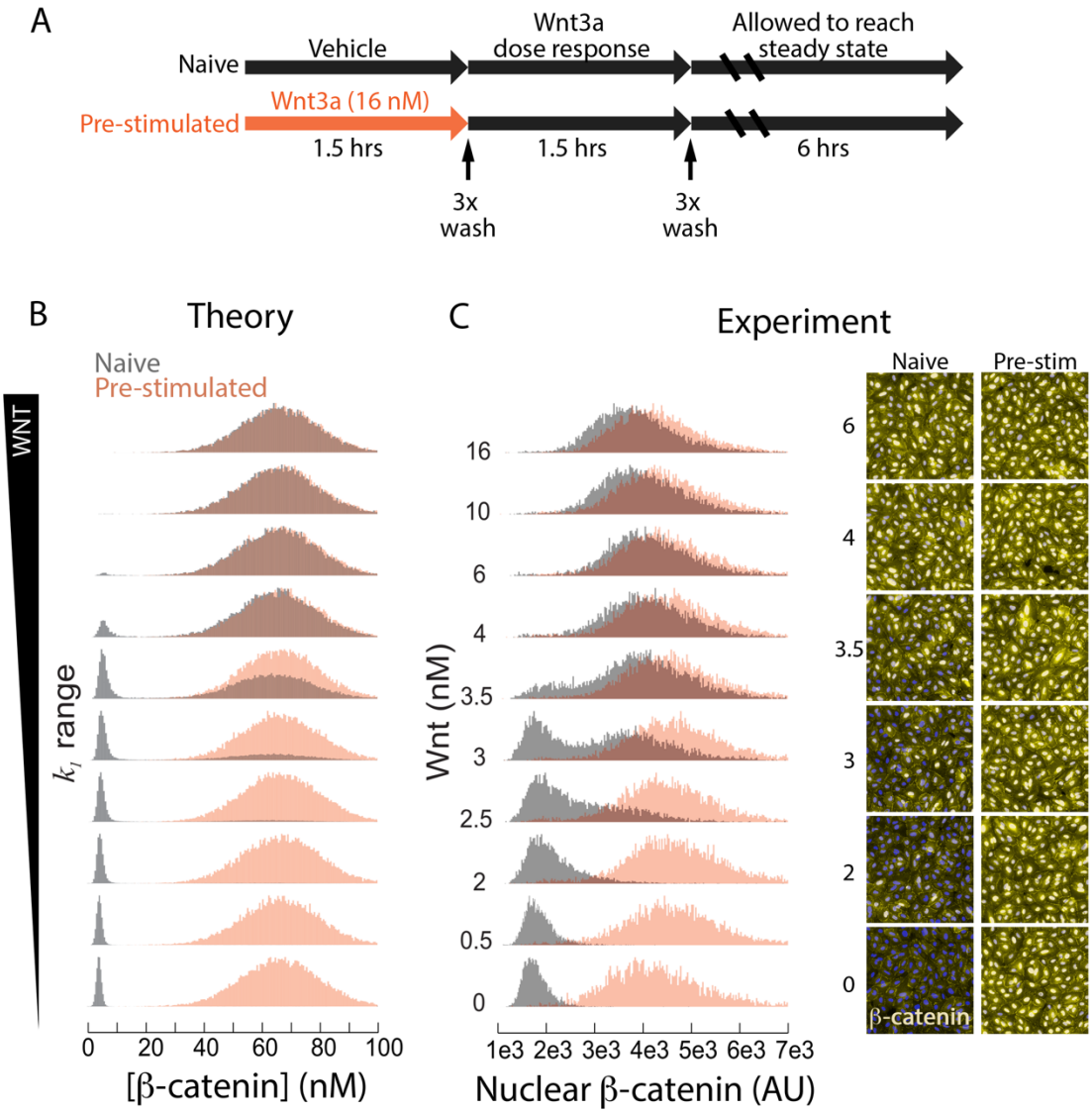

342

Figure 5

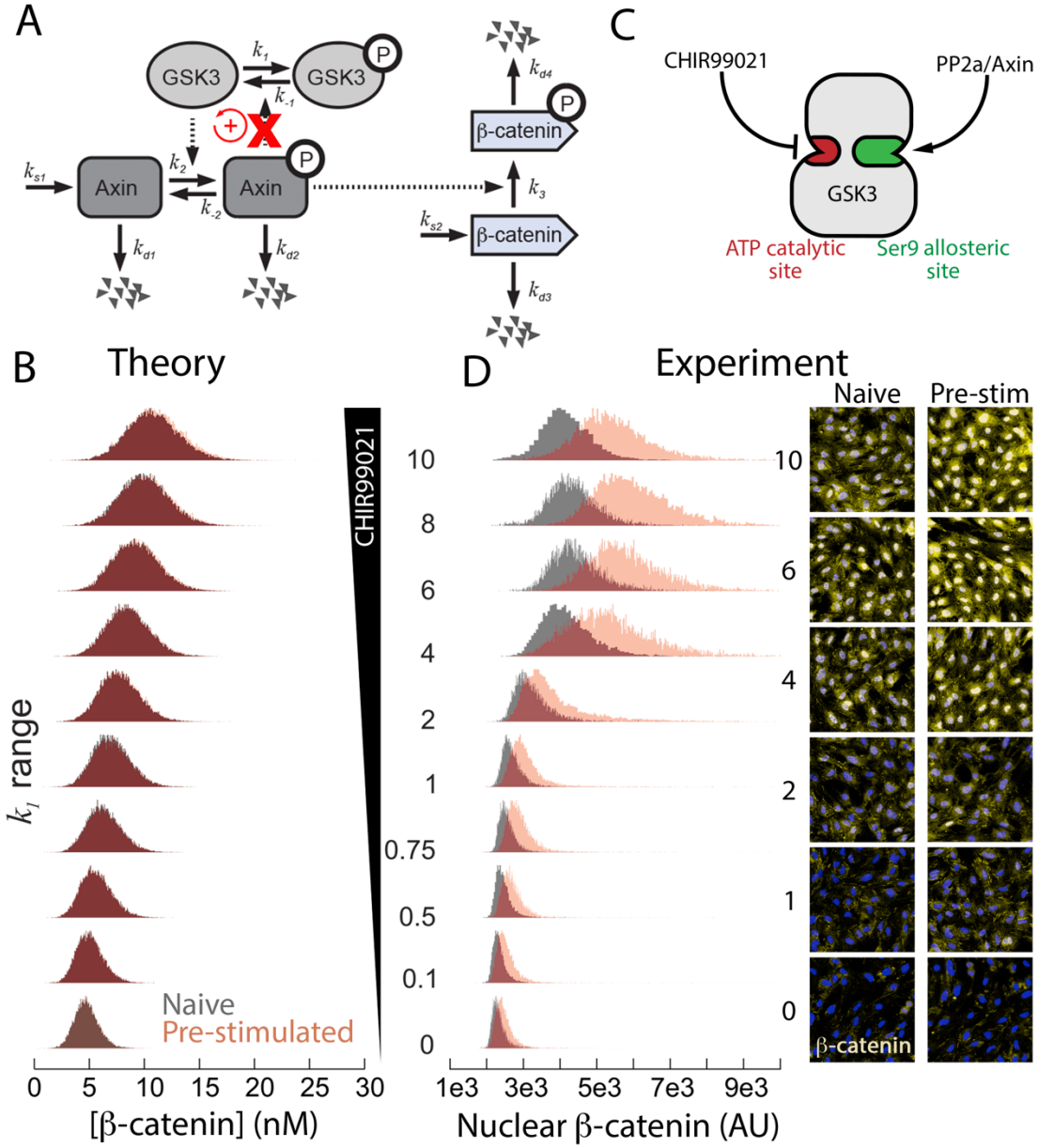

343

Supplementary Materials for

Feedback in the β-catenin destruction complex imparts bistability and cellular memory

Authors: Mary Jo Cantoria, Elaheh Alizadeh, Janani Ravi, Nawat Bunnag, Arminja N. Kettenbach, Yashi Ahmed, Andrew L Paek, John J. Tyson, Konstantin Doubrovinski, Ethan Lee, Curtis A. Thorne

Materials and Methods

Plasmids and radiolabeled proteins

Radiolabeled β-catenin and Axin were generated in rabbit reticulocyte lysates (Promega) according to the manufacturer's instructions. Degradation assays were performed based on previously published methods (*7, 25*).

Xenopus extract studies

Xenopus embryos were *in vitro* fertilized, dejellied and extracts prepared as previously described (*7*).

Immunoblots

Cells were lysed in non-denaturing buffer (50 mM Tris-Cl, pH 7.4, 300 mM NaCl, 5 mM EDTA, 1% w/v Triton X-100) and the soluble fraction was used for immunoblotting. For Axin immunoblots, Axin was immunoprecipitated with mouse anti-Axin antibody (Zymed) and immunoblotted with anti-Axin 1 goat antibody (R & D). Total GSK3 and GSK3 pS21 (Cell

366 Signaling) were detected from lysates denatured in lysis buffer containing 1% SDS, protease and
367 phosphatase inhibitors.
368
369 Kinase assays
370 *In vitro* kinase assays were performed as previously described (*14*).
371
372 Cell Culture
373 HEK293 were purchased from ATCC and cultured based in ATCC protocols. Human colonic
374 epithelial cells (HCECs) were cultured in 5% CO_2 in DMEM supplemented with 10% FBS, 1x
375 penicillin-streptomycin and 1x glutamax.
376
377 Bistability experiments
378 HCECs were plated at 20,000 cells/well in fluorescent 96-well plates (Greiner Bio-One;
379 Cat#655090) on day 0. Cells were incubated and allowed to reach 100% confluence. On day 2,
380 cells were treated with increasing concentrations of recombinant human Wnt3A (R&D; Cat#5036-
381 WN-500, with carrier) for 1.5 h. Cells were then washed with PBS thrice and complete media
382 (DMEM high glucose containing 10% FBS, 1x glutamax and 1x penicillin-streptomycin) was
383 added. Cells were incubated for 3 h and fixed with 4% paraformaldehyde-sucrose solution.
384
385 Hysteresis: HCECs were plated at 20,000 cells/well in fluorescent 96-well plates (Greiner Bio-
386 One; Cat#655090) on day 0 and allowed to reach 100% confluence on day 2. HCECs were treated
387 with Wnt3a long enough to stimulate the pathway (1.5 h), but short enough to avoid negative
388 feedback from the destruction complex ($\leq$ 6 h) (Fig. S6) by Axin2, a transcriptional target of the

Wnt pathway. Cells were treated either without (Naive) or with 16 nM of Wnt3A (Pre-stimulated) for 1.5 h. Cells were washed with PBS three times and subsequently treated with increasing concentrations of Wnt3A for 1.5 h. Cells were washed with PBS three times, replaced with complete media for 3 h and fixed.

Stimulation through direct GSK3 inhibition (Fig 5): HCECs were plated as described above. In Fig. S7, cells were treated with CHIR99021 at the indicated concentrations and durations. We chose the concentration of 10 μM for 6h because with these conditions the β-catenin response reached steady state. Cells were treated with increasing concentrations of CHIR99021 (Selleck Chemicals; Cat#S1263) for 6 hrs and then fixed. For the hysteresis experiment using CHIR99021: HCECs were plated as above. On day 2, cells were treated with either DMSO (Naive) or 10 μM of CHIR99021 (Pre-stimulated) for 6 hrs. Cells were washed with PBS three times, treated CHIR99021 dose curve for 6 hrs and fixed.

Immunofluorescence

Fixed cells were permeabilized with 0.2% Triton X-100, blocked with 2.5% BSA, and stained with β-catenin antibody at 1:300 (BD Biosciences; Cat#610154) diluted in 2.5% BSA. After washing with PBST (0.1% Tween-20), cells were incubated in secondary antibody conjugated to 1:1000 Alexa fluor (Invitrogen; Cat#A1103) diluted in 2.5% BSA for 2 hrs in the dark. Cells were washed in PBST and DAPI was used to stain nuclei. Cells were imaged on Perkin Elmer Operetta System using a 20x air objective.

Nuclear image segmentation

412 To isolate single cell data, nuclear segmentation was performed using the Perkin Elmer Harmony
413 software as previously described (*26*). β-catenin nuclear intensity was normalized to nuclear area
414 of each cell (nuclear β-catenin). Data analysis codes were custom-built using R.
415
416 Mathematical modeling
417 To better understand sufficiency requirements for the emergence of bistability in our system, we
418 developed a minimal mathematical model of the Wnt pathway dynamics. Our equations describe
419 the dynamics of concentrations of Axin, GSK3, and β-catenin in both their phosphorylated and
420 unphosphorylated states. Intermolecular interactions accounted for in the model follow directly
421 from Fig. 2A. Specifically, we assume that Axin is phosphorylated at a rate that increases with the
422 concentration of unphosphorylated GSK3, whereas GSK3 is dephosphorylated at a rate that
423 increases with the concentration of phosphorylated Axin. We further assume that β-catenin is
424 phosphorylated at a rate proportional to the concentration of phosphorylated Axin, which leads to
425 its rapid depletion (since the rate of phospho-β-catenin degradation is assumed to be much higher
426 than that of its unphosphorylated form). Additionally, Axin and β-catenin are produced at constant
427 rates. Finally, Axin and β-catenin undergo degradation in both their phosphorylated and
428 unphosphorylated forms.
429
430 Dynamical equations that define our model follow straightforwardly from the above assumptions
431 and are given in Table S1. To analyze the model, we first note β-catenin concentration dynamics
432 do not feedback on the dynamics of the other molecules. In this way, the behavior of β-catenin is
433 a readout of the state of the pathway and need not be considered when examining the nature of its
434 possible dynamical states. Additionally, the total amount of GSK3 is constant (see Eq 4) since its

435 degradation is negligible on the timescale of our experiment (*10*). Thus, three dynamical equations
436 (specifying the dynamics of Axin, phospho-Axin, and unphosphorylated GSK3) suffice to specify
437 the behavior of model uniquely (see Table S1, Eq 1-3).
438
439 The key feature of the model is a positive feedback loop between GSK3 dephosphorylation and
440 Axin phosphorylation. Specifically, the rate of GSK3 dephosphorylation increases with the
441 concentration of phosphorylated-Axin (V_{-1} term), whereas the rate of Axin phosphorylation
442 increases with the concentration of (unphosphorylated) Axin (V_2 term). The activity of the pathway
443 regulates the levels of β-catenin through phosphorylation of β-catenin (V_3 term) which is thereby
444 targeted for proteasomal degradation (V_{d4} term). The other terms account for Axin-independent
445 phosphorylation of GSK3 (V_1 term), GSK3-independent Axin dephosphorylation (V_{-2} term), de
446 novo translation of Axin (V_{s1} term) and β-catenin (V_{s2} term), and spontaneous "background"
447 degradation of Axin in its phosphorylated and unphosphorylated states (V_{d2} and V_{d1} terms
448 respectively) as well as that of β-catenin in its unphosphorylated state (V_{d3} term).
449
450 In the simplest initial version of the model, it was assumed that no cooperativity was present in
451 any reaction step such that the terms V_2 and V_{-2} were linear in $[GSK3]$ and $[Axin^p]$ respectively.
452 Setting all time-derivatives to zero, these equations are readily solved for the steady state
453 concentrations (which we did using symbolic algebra software Maple, Maplesoft) to obtain two
454 steady state solutions. Setting all time-derivatives to zero, these equations are readily solved for
455 the steady state concentrations (which we did using symbolic algebra software Maple, Maplesoft)
456 to obtain two steady state solutions, one of which is stable and the other unstable. This result
457 indicates that the simplest version of the equations cannot exhibit bistability since bistability

458 requires the coexistence of three steady state solutions (two stable and one unstable). That the
459 simple version of the model does not exhibit bistability can be established rigorously by
460 applying chemical reaction network theory (CRNT) [The Chemical Reaction Network Toolbox,
461 Windows Version | Zenodo].
462
463 Hence, to explain bistability, we modified the model to account for the possible presence of
464 cooperativity in both Axin phosphorylation by GSK3 as well as in its dephosphorylation. We note
465 these are assumptions; however, our analysis shows that cooperativity in (at least some of the)
466 intermolecular interactions is required to generate bistable dynamics. The equations are still
467 possible to solve analytically, though the solutions are quite lengthy and thus not presented here.
468 Accounting for possible presence of cooperativity does lead to three solution branches, as indicated
469 in the bifurcation diagram in Fig. S2. To explore the stability of the different branches, we
470 performed numerical simulations where our dynamical equations were solved using an explicit
471 Euler forward scheme. We found that in an open set of parameter values, two stable branches can
472 co-exist with an unstable branch thus implying that our minimal model can account for bistability
473 of the pathway (Fig. S2).
474
475 In our minimal model, a steady state with zero concentrations of both phospho-Axin and
476 unphosphorylated GSK3 is present for all values of model parameters. Arguably, this feature is
477 non-generic since it is not present when phospho-GSK3 can be dephosphorylated spontaneously
478 (in the absence of phospho-Axin). However, our model is a good approximation of this later
479 situation if the rate of spontaneous GSK3 dephosphorylation is negligible. It may be shown that a
480 small rate of spontaneous GSK3 dephosphorylation will change the appearance of the bifurcation
481 diagram in Fig. S2 to produce a single root locus where two saddle-node bifurcations are connected

by an unstable branch. For high rates of spontaneous GSK3 dephosphorylation, bistability is lost and only a single stable branch will remain. These predictions are in principle testable, provided one can control the rate of GSK3 dephosphorylation for example by a phosphatase, presumably PP2a. However, this work is beyond the scope of the present study.

To further examine the dynamics of the pathway and to more closely compare theoretical predictions to experimental results, we examined the response of the pathway to quasi-static variation of a control parameter. Specifically, we varied the rate of spontaneous GSK3 phosphorylation (k_1) and examined the resulting steady-state concentration of β-catenin. This was done using two procedures that we term "Naive" and "Pre-stimulated". In the former case, the value of k_1 was initially set to a low value and was then increased quasi-statically. In the latter case, k_1 was gradually decreased, starting with a large initial value. Fig. 2 shows the plots of the steady-state β-catenin levels as a function of k_1 corresponding to the two simulated protocols. It is seen that the two curves do not coincide, indicating the presence of hysteresis. Specifically, in the Pre-stimulated case when k_1 was large initially, the initial levels of β-catenin were correspondingly high and remained high for a substantial range of (decreasing) k_1 values. In the Naive case, when k_1 was increased from a value initially set to be low, steady-state β-catenin levels remained much lower than seen in the Pre-stimulated case (for the same values of k_1). This hysteretic behavior is a key hallmark of bistability and is readily anticipated from the phase portrait given in Fig. S2.

We next asked if our minimal computational model can interpret our observations on the distribution of Wnt pathway activation levels in cell populations (Fig. 3D, 4C, 5D). Clearly, the precise level of nuclear β-catenin varies from cell to cell. To capture this variation, we considered

an ensemble of cells, with each cell having a different random value of spontaneous GSK3 phosphorylation k_1. Expectedly, this results in a stochastic distribution of steady-state β-catenin levels. Next, we examined changes in the simulated distribution of pathway activation as the mean value of k_1 was varied according to the two protocols described above and as shown in Fig. 2. We found that the distribution of β-catenin levels becomes bimodal within a finite intermediate range of the mean k_1 values. This is another key hallmark of bistability and is in complete agreement with the experimental data (see Fig. 4B and 4C). At the same time, average β-catenin levels follow the same qualitative trend as was seen in Fig. S9, where the deterministic dynamics without stochastic variation in k_1 were examined. Finally, we asked if the dynamics of the pathway may be rendered monostable by means of perturbations that interfere with the positive feedback between Axin and GSK3. To this end, we made the rate of Axin phosphorylation independent of GSK3 concentration. In this case, the dynamics became monostable such that no hysteresis was seen when k_1 was first increased and then decreased quasi-statically, see Fig. S9E.

To account for the effect of Wnt stimulation on the pathway, we considered four alternative scenarios. Specifically, in our model, Wnt can stabilize β-catenin by 1) increasing k_1 , 2) decreasing k_{-1}, 3) increasing k_{-2} or 4) decreasing k_2. Expectedly, in all these cases, the system exhibits hysteresis (Fig. S9), since, generically, the presence of hysteresis does not depend on the particular choice of the control parameter (as long as varying the control parameter allows to move from a bistable to a monostable regime).

Table S1: Set of ordinary differential equations for the system in Fig. 2A.

$$\frac{d[Axin]}{dt} = -V_2 + V_{-2} - V_{d1} + V_{s1} \qquad (1)$$

528 $$\frac{d[Axin^p]}{dt} = +V_2 - V_{-2} - V_{d2} \quad (2)$$

529 $$\frac{d[GSK3\beta]}{dt} = -V_1 + V_{-1} \quad (3)$$

530 $$[GSK3\beta] + [GSK3\beta^p] = GSK3\beta_{tot} = constant \quad (4)$$

531 $$\frac{d[\beta catenin^p]}{dt} = V_3 - V_{d4} \quad (5)$$

532 $$\frac{d[\beta catenin]}{dt} = V_{s2} - V_{d3} - V_3 \quad (6)$$

533

534 **Table S2: Reaction rates for the model.**

535 $V_1 = k_1\,[GSK3\beta]$

536 $V_{-1} = k_{-1}\,([GSK3\beta_{Tot}] - [GSK3\beta])[Axin^p]$

537 $V_2 = k_2[GSK3\beta]^2[Axin]$

538 $V_{-2} = k_{-2}[Axin^p]^2$

539 $V_{d1} = k_{d1}[Axin]$

540 $V_{d2} = k_{d2}[Axin^p]$

541 $V_{s1} = k_{s1}$

542 $V_{d4} = k_{d4}[\beta catenin^p]$

543 $V_3 = k_3[\beta catenin][Axin^p]$

544 $V_{s2} = k_{s2}$

545 $V_{d3} = k_{d3}[\beta catenin]$

546

547 **Table S3: Rate constants used in the model.**

Variable	Value	Definition	Ref

k_{s1}	$8.2x10^{-5}$ nM min^{-1}	Axin synthesis rate	(*10*)
k_{d1}	0.167 min^{-1}	Axin degradation rate constant	(*10*)
k_{d2}	0.004 min^{-1}	$Axin^{p}$ degradation rate constant	Assumption
k_1	Fig S9A & Fig 2B : 0.05-2 [min^{-1}] Fig S9B: 1[min^{-1}] Fig. S9C: 1[min^{-1}] Fig. S9D: 1[min^{-1}] Fig. S9E & Fig 2C: 0.05-4[min^{-1}]	phosphorylation rate of GSK3	
k_{-1}	Fig S9A & Fig 2B : 1 [nM^{-1} min^{-1}] Fig S9B: 0.05-4 [nM^{-1} min^{-1}] Fig. S9C:1 [nM^{-1} min^{-1}] Fig. S9D:2 [nM^{-1} min^{-1}] Fig. S9E & Fig 2C:0.001 [min^{-1}]	Dephosphorylation rate of $GSK3^{p}$	
k_2	Fig S9A & Fig 2B : 2 [nM^{-2} min^{-1}] Fig S9B: 2[nM^{-2} min^{-1}] Fig. S9C:0.05-10 [nM^{-2} min^{-1}] Fig. S9D: 2[nM^{-2} min^{-1}] Fig. S9E & Fig 2C: 2[nM^{-2} min^{-1}]	phosphorylation rate of Axin	
k_{-2}	Fig S9A & Fig 2B : 2 [nM^{-1} min^{-1}] Fig S9B: 2[nM^{-1} min^{-1}] Fig. S9C:2 [nM^{-1} min^{-1}] Fig. S9D: 0.05-10 [nM^{-1} min^{-1}] Fig. S9E & Fig 2C: 2[nM^{-1} min^{-1}]	Dephosphorylation rate of $Axin^{p}$	

k_3	$5nM^{-1}\ min^{-1}$	Phosphorylation rate of β-catenin	Assumption
k_{s2}	$0.42\ nM\ min^{-1}$	Synthesis rate of β-catenin	(*10*)
k_{d3}	$6.3x10^{-3}\ min^{-1}$	Degradation rate of βcatenin	(*10*)
k_{d4}	$0.42\ min^{-1}$	Degradation rate of β-catenin^p	(*10*)
$GSK3_{Tot}$	50nM	Total concentration of GSK3	(*10*)

Table S4: Two initial conditions used to solve the ODEs.

Experiment[nM]	Axin	Axin^p	GSK3	βcatenin	βcatenin^p
Naive	4×10^{-4}	5×10^{-3}	50	1	30
Pre-stimulated	6.1×10^{-4}	1×10^{-6}	2	30	1

Fig S1. (**A**) Cartoon of Axin SLiM site mutant effect on GSK3 activation. (**B**) Alignment of the B56 binding site sequence in four species reveals strong evolutionary conservation.

Fig S2. Solving the ODEs analytically leads to three fixed points. We explored the stability of the different branches using numerical simulations where our dynamical equations were solved. Two of the fixed points were stable and can co-exist while the third fixed point was unstable.

Fig S3. To account for heterogeneity of the cells, we ran the simulation for 2000 cells and in each

559 run we randomly choose a k_1 value from a normal distribution instead of a single value. (**A**) Range
560 of k_1 used for the model in which there is a positive feedback loop and bistability response is
561 observed as shown in Fig. 3B and Fig. 4B. (**B**) Range of k_1 used for the model where the positive
562 feedback loop is broken, and we see a graded response as shown in Fig. 5D.
563
564 **Fig S4.** Plot of mean β-catenin response to increasing and decreasing Wnt3a stimulation from Fig.
565 3D, (EC_{50}= 3.78 nM; n_H = 6.35).
566
567 **Fig S5.** Plot of mean β-catenin response to increasing and decreasing Wnt3a stimulation from Fig.
568 4D.
569
570 **Fig S6.** (**A**) HCECs were treated with recombinant Wnt3a (16 nM) for one hours, washed three
571 times and regular growth media minus Wnt3a was added back. Nuclear β-catenin is plotted.
572 Nuclear β-catenin remains high at 6 h after removal but afterward comes back down. (**B**) HCECs
573 were treated with different concentrations of the CHIR99021 for various durations. Cells were
574 allowed to reach steady-state using nuclear localization of β-catenin as a readout. The effect of
575 CHIR99021 on nuclear β-catenin localization in HCECs is reversible 3h after removal of the
576 compound. CHIR99021 was used at 10 μM concentration for six hours.
577
578 **Fig S7.** (**A**) HCECs were treated with different concentrations of GSK3i CHIR99021 for various
579 durations. Nuclear localization of β-catenin is plotted. β-catenin steady state was achieved at 6
580 hours under sustained CHIR99021 stimulation. (**B**) β-catenin hysteresis experiment was performed
581 with identical treatment times as was described in Fig. 4A, except CHIR99021 was used instead

582 of Wnt3a. Unlike the effect observed in cells treated with Wnt3a, cells treated with CHIR99021
583 cannot maintain memory of the stimulation and return to basal β-catenin concentrations at the 6 hr
584 timepoint.
585
586 **Fig S8.** Plot of mean β-catenin response to increasing and decreasing CHIR99021 stimulation from
587 Fig. 5D.
588
589 **Fig S9.** We assumed four different scenarios where in each scenario one of k1, k2, k-2, and k-1
590 rate constants changes and the others remain constant with increasing Wnt. (**A**) Wnt increases k1
591 with k_2=2, k2=2, and k_1=1. (**B**) Wnt decreases k-1 with k_2=2, k2=2, and k1=1. (**C**) Wnt
592 decreases k2 with k_2=2, k1=1, k_1=1. (**D**) Finally Wnt increases k-2 with k2=2, k1=1,k_1=2. As
593 shown in these four panels for a range of these parameters we see bistability in the concentrations
594 of the molecules. (**E**) We simulated adding GSK3i as disrupting the positive feedback loop and
595 leading to a graded response in β-catenin concentration rather than a bistable response.
596
597
598

Fig S1

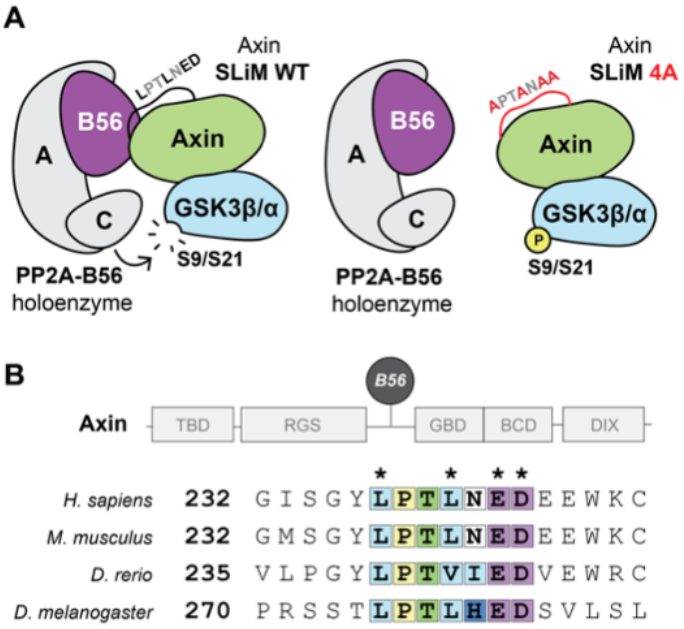

599

Fig S2

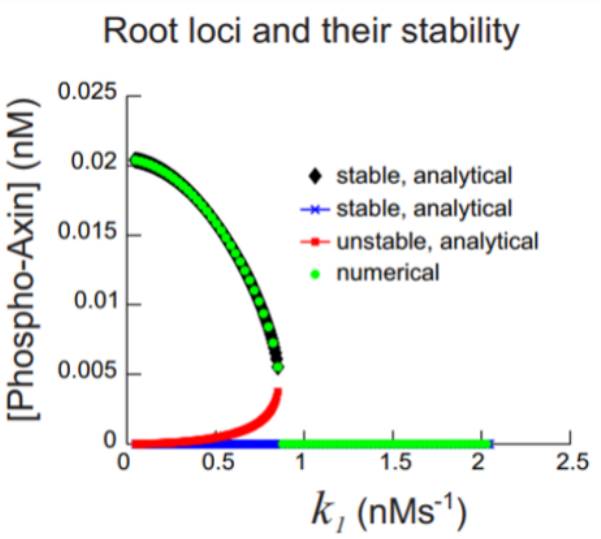

600

Fig S3

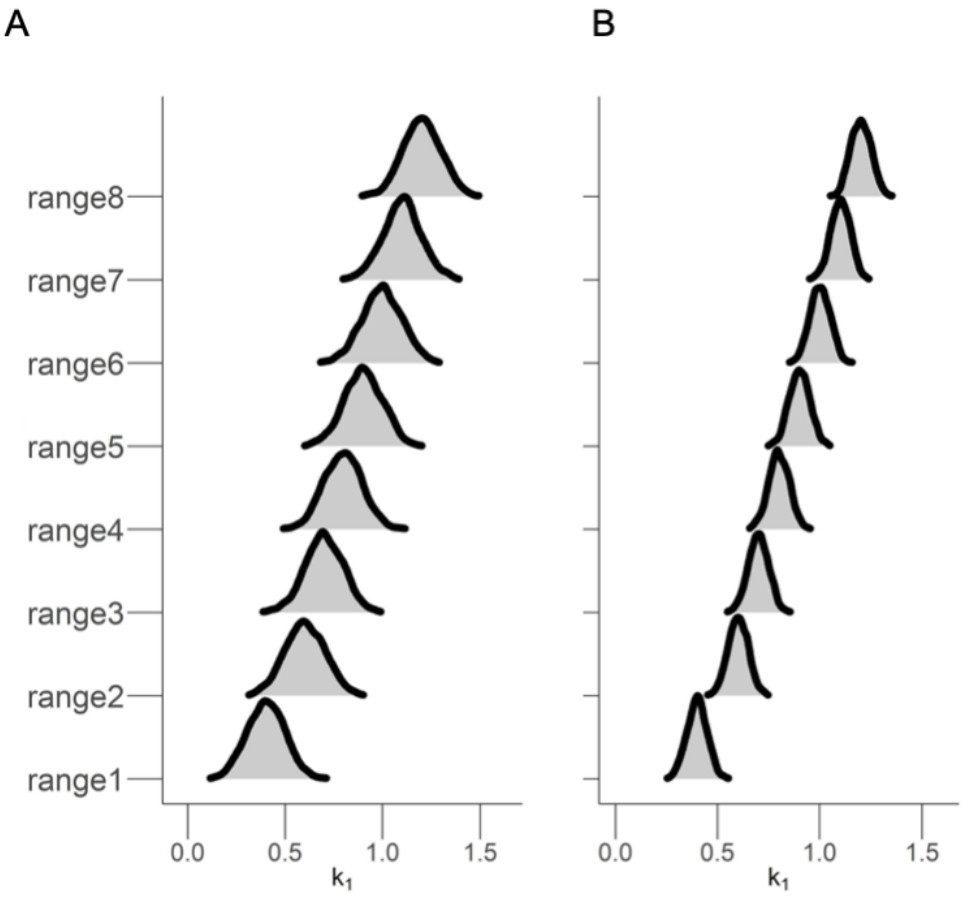

601

Fig S4

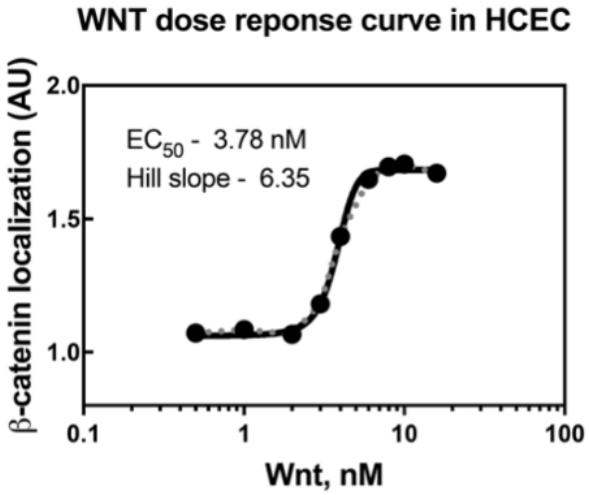

602

Fig S5

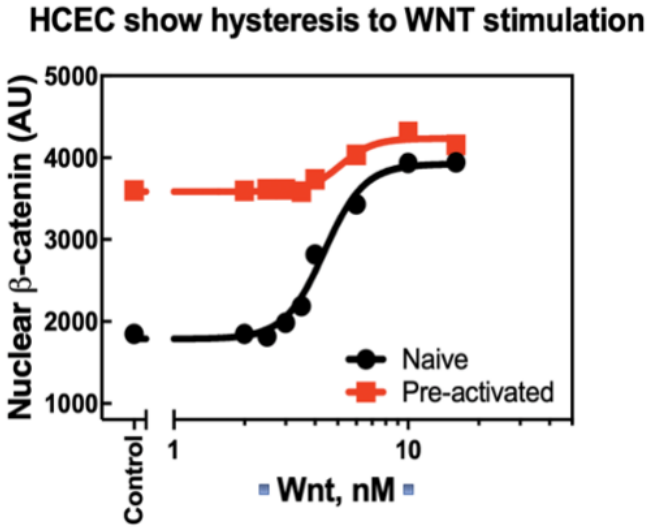

603

Fig S6

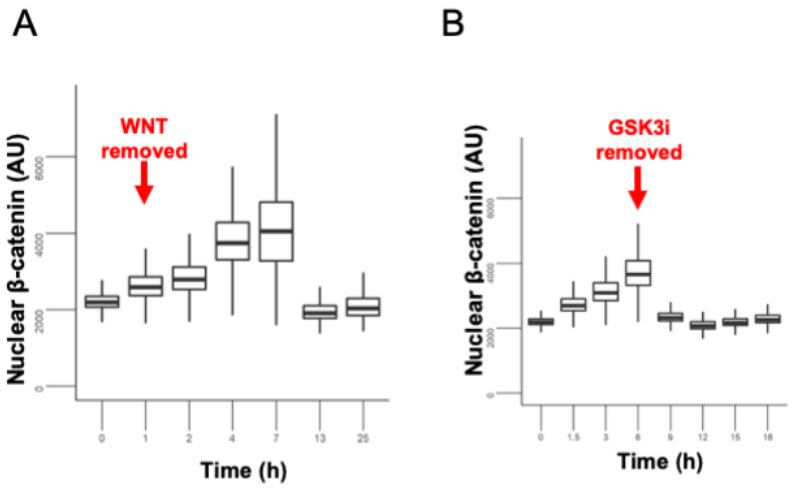

604

Fig S7

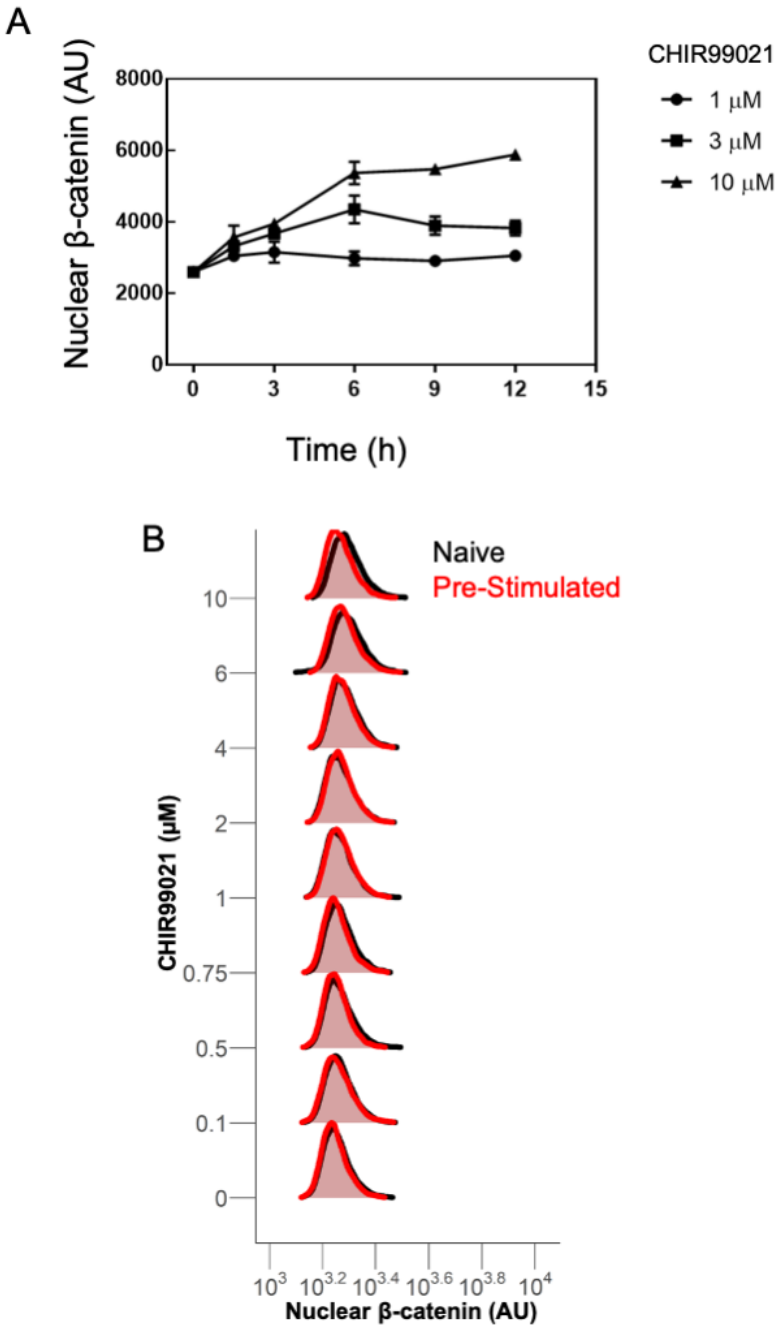

605

Fig S8

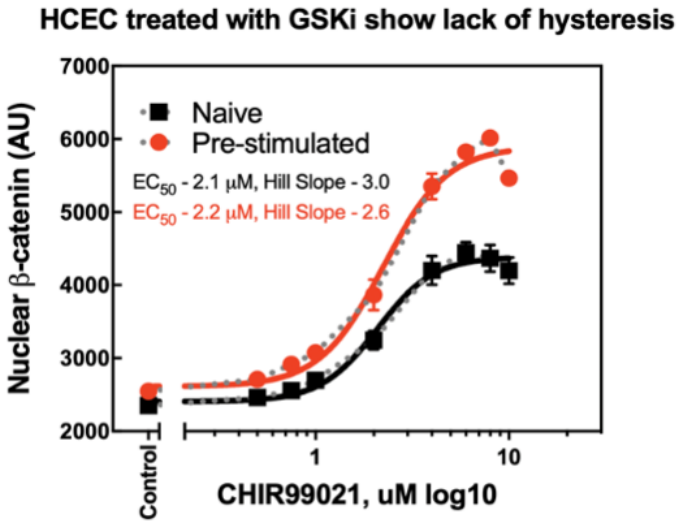

606

Fig S9

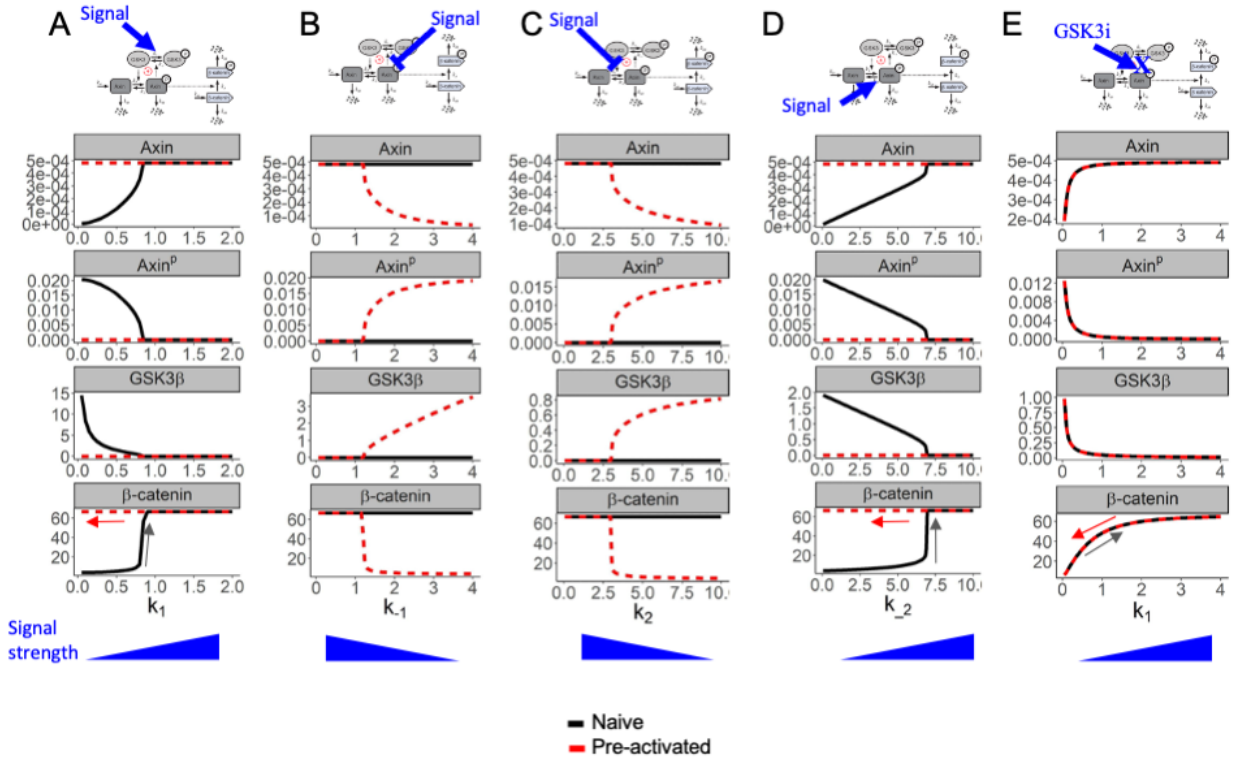

607

608